

1 **Modeling ground deformations of Panarea volcano hydrothermal/geothermal system**
2 **(Aeolian Islands, Italy) from GPS data.**

3

4 Alessandra Esposito ^a, Marco Anzidei ^a Simone Atzori ^a, Roberto Devoti ^a, Guido Giordano ^b,
5 Grazia Pietrantonio ^a

6

7 ^a Istituto Nazionale di Geofisica e Vulcanologia, Via di Vigna Murata 605, 00143 Roma Italy.

8

9 ^b Dipartimento Scienze Geologiche, Università Roma Tre, L.go S. L. Murialdo 1, 0146 Rome,

10 Italy

11

12

13 Corresponding author

14 E-mail address: alessandra.esposito@ingv.it (Alessandra Esposito); +39 06 51860 217; fax

15 +39 06 504 13 03

16

17 **Abstract**

18 Panarea volcano (Aeolian Islands, Italy) was considered extinct until November 3, 2002 when
19 a submarine gas eruption began in the area of the islets of Lisca Bianca, Bottaro, Lisca Nera,
20 Dattilo and Panarelli, about 2.5 km east of Panarea Island. The gas eruption decreased to a
21 state of low degassing by July 2003.

22 Before 2002 the activity of Panarea volcano was characterized by mild degassing of
23 hydrothermal fluid. The compositions of the 2002 gases and their isotopic signatures
24 suggested that the emissions originated from a hydrothermal/geothermal reservoir fed by
25 magmatic fluids.

26 We investigate crustal deformation of Panarea volcano using the GPS velocity field obtained
27 by the combination of continuous and episodic site observations of the Panarea GPS network
28 in the time span 1995-2007.

29 We present a combined model of Okada sources which explains the GPS results acquired in
30 the area after December 2002. The kinematics of Panarea volcano show two distinct active
31 crustal domains characterized by different styles of horizontal deformation, supported also by
32 volcanological and structural evidences. A subsidence in the order of several mm/yr is
33 affecting the entire Panarea volcano and a shortening of 10^{-6} yr⁻¹ has been estimated in the
34 Islets area.

35 Our model reveals that the degassing intensity and distribution are strongly influenced by
36 geophysical-geochemical changes within the hydrothermal/geothermal system. These
37 variations may be triggered by changes in the regional stress field as suggested by the
38 geophysical and volcanological events that occurred on 2002 in the Southern Tyrrhenian area.

39

40 Key words: GPS monitoring, model, gas eruption, active volcanism, Aeolian arc.

41 **1. Introduction**

42 Crustal deformation measurements are among the most sensitive and reliable indicators to
43 evaluate the volcanic hazard related to volcanic unrests (Dvorak and Dzurisen, 1997) caused
44 by magma emplacement and/or fluid migration (Gottsmann et al., 2007). A clear link for the
45 hydrothermal fluid contribution to geophysical signals has been found in several volcanoes
46 (Todesco et al., 2004; Tikku et al., 2006) .

47 On November 3 2002, a gas eruption began about 2.5 km offshore, east of Panarea Island
48 (Aeolian Islands, Italy). Submarine craters opened at the top of a 2.3 km² shallow rise of the
49 seafloor, between -2 m and -30 m below sea level in the area surrounded by the islets of
50 Panarelli, Lisca Bianca, Bottaro, Lisca Nera and Dattilo (hereinafter as the “Islets area”)
51 (Figure 1) (Anzidei et al., 2003a, 2003b; Esposito et al., 2006). The degassing of Panarea on
52 November 3rd followed a sequence of geophysical and volcanological events which occurred
53 in the southern Tyrrhenian zone (Anzidei et al. 2003b; Esposito et al., 2006): the offshore
54 earthquake (Ml=5.6) between Palermo and Ustica Island on September 6th, the onset of the
55 paroxysmal eruption at Mt Etna on October 27th and the eruption at Stromboli that started on
56 December 28th (Figure 1 a).

57 Until November 2002, the presence of a hydrothermal/geothermal system at Panarea was
58 interpreted in terms of post-volcanic phenomena caused by fluid circulation due to cooling of
59 a magmatic source (Romano 1973; Bellia et al.,1986; 1987; Gabbianelli et al., 1990; Italiano
60 and Nuccio, 1991; Calanchi et al., 1995, Anzidei, 2000). A deep and a shallow zone were
61 recognized (Italiano and Nuccio 1991; Calanchi et al. 1995). However, gas eruptions of
62 similar intensity to the 2002 eruption had not been previously observed during the last century
63 (Mercalli, 1883). Gas compositions and isotopic signatures suggested that the 2002 emissions
64 originated from a hydrothermal/geothermal reservoir fed by sea water and magmatic fluids

65 (Caliro et al., 2004; Chiodini et al., 2006; Capaccioni et al., 2005, 2007). Geomorphological
66 evidence of past phreatic explosions, like that of November 2002, have been found in the
67 relics of several craters on the seafloor, revealed by multibeam bathymetry (Anzidei et al.,
68 2005), as well as by geological investigations (Esposito et al., 2006). Intense hydrothermal
69 activity is also evident in the Islets area.

70 Prior to the 2002 event one GPS station was present on Panarea Island as part of Tyrgeonet
71 Mediterranean GPS network (Anzidei et al., 1995) After November 2002, a dedicated GPS
72 network was planned and set up to monitor the short-term surface and subsurface dynamics at
73 Panarea volcano. In this paper we show and discuss results from GPS data from 1995 to 2007
74 which include the discontinuous data from the single station for the pre-eruption period and
75 seven non-continuous and two continuously monitoring stations for the post-eruption period.
76 We estimate the active strain and discuss the relationship between the deformation processes
77 related to the hydrothermal/geothermal system and the regional and local tectonic setting. We
78 use an elastic Okada model to fit the GPS velocity field to explain the present evolution of the
79 hydrothermal/geothermal system in the post eruption stage.

80

81 **2. Structural and Volcanic setting**

82 Panarea Island is located on the eastern sector of the Aeolian volcanic arc, located along the
83 margin of the Southern Tyrrhenian Sea, facing the Calabrian-Peloritan mountain chain to the
84 south-east and the abyssal Marsili basin to the north-west (Barberi et al., 1973, Beccaluva et
85 al., 1985). The Aeolian volcanoes comprise of seven major islands (Alicudi, Filicudi, Salina,
86 Lipari, Vulcano, Panarea and Stromboli), and several seamounts (Figure 1 a) emplaced on a
87 15 - 20 Km thick continental crust. Their products have been dated between 1.3 Myr and the
88 present (De Astis et al., 2003 and reference therein). Volcanism started during the Pliocene, in

89 connection with the subduction of the Ionian lithosphere beneath the Calabrian Arc.
90 Structural, seismological, geodetic and geochemical data suggest that since the Pleistocene,
91 the south-eastern propagation of the Tyrrhenian rifting and the western margin roll-back have
92 been controlled by the NNW-SSE fault system (Tindari-Letojanni fault system) and different
93 styles of rifting processes have been recognized (Gvirtzman and Nur, 1999; 2001; Faccenna et
94 al., 2001; De Astis et al., 2003). Recent regional geodetic data show maximum strain
95 contraction axes with a N-S trend off of Sicily and in the western portion of the Aeolian
96 Islands and a minor NW-SE extension in the eastern Aeolian Islands (Hollenstein et al., 2003;
97 Pondrelli et al., 2004; D'Agostino and Selvaggi, 2005, Esposito, 2007). The transition from
98 compressional to extensional regime happens through an area with transtensional deformation
99 clustering along the NNW-trending Tindari-Letojanni fault system which runs across the
100 central Aeolian Islands (Pondrelli et al. 2004; D'Agostino and Selvaggi, 2005, Serpelloni et
101 al., 2005; Esposito, 2007). Panarea Island is located on the eastern active sector of the Aeolian
102 volcanic arc which also includes Stromboli Island and the Lamentini, Alcione and Palinuro
103 seamounts. A prevailing NNE- to NE trending fault system affects the Panarea and Stromboli
104 Islands (Gabbianelli et al., 1993; De Astis et al., 2003; Tibaldi et al., 2003).
105 Panarea volcano is the emergent portion of a submarine stratovolcano ~ 1600 m high and ~18
106 km across (Gabbianelli et al., 1993; Gamberi et al., 1997; Favalli et al., 2005) characterized by
107 a large and ellipsoidal shaped platform, at ~100 m. The emergent portion of this platform
108 forms Panarea Island (421 m a.s.l.) and the small archipelago with the islets of Basiluzzo,
109 Dattilo, Panarelli, Lisca Bianca, Bottaro, Lisca Nera and Le Formiche. Panarea and the Islets
110 are made of high-K calcalkaline, andesite to dacite and rhyolite rocks, lava domes, plugs,
111 coulees and lava flows, interbedded with subordinated pyroclastic deposits also of external
112 provenance. Age ranges from 149 ± 5 to 54 ± 8 ka (Calanchi et al., 1999; Lucchi et al., 2007).

113 Recently, the youngest age of the Panarea dome complex was determined at 20 ± 2 ka (Dolfi
114 et al., 2007). The outcropping lava units on the Islets area are characterized by a variable
115 degree of hydrothermal alteration that have heavily modified their mechanical parameters
116 (Cas et al., 2007).

117 Gravimetric measurements revealed the existence of a positive local gravimetric anomaly
118 between the islet of Basiluzzo and the island of Panarea (Gabbianelli et al., 1990). Cocchi et
119 al. (2008) estimated a negative magnetic anomaly between Panarea and the Islets area. In the
120 Islets area a positive residual magnetic anomaly is present. A NE-trending gravity minimum,
121 centered on the west of Panarea was also measured (Cocchi et al., 2008).

122 Before November 2002, Panarea volcano had been undergoing active subsidence at 1.87 mm
123 yr^{-1} for the last 2000 years (Tallarico et al. 2003) and continuous exhalative activity from
124 several fumaroles located both inland and offshore (La Calcara, Punta Levante and Lisca
125 Bianca – Bottaro, in Figure 1).

126 Panarea volcano shows faults and fractures with a prevailing NE-NNE-trend and minor NW-
127 trend (Gabbianelli et al., 1990, 1993; De Astis et al., 2003). During the 2002 gas eruption
128 (Anzidei et al., 2005; Esposito et al., 2006, 2008) two fracture systems opened on the seafloor
129 in the degassing area: NNE-SSW and NW-SE trending (Anzidei et al., 2005; Esposito et al.,
130 2006; 2007).

131

132 **3. GPS networks and data analysis**

133 The Panarea GPS network includes seven non-continuous stations and two continuous stations
134 (Figure 2). Two of the non-continuous stations are located on Panarea Island (PANA-PA3D;
135 PCOR) and the others on the Islets area (BA3D, LIBI, BOTT, LINE, and PNRL) (Figure 2
136 and Table 1) (Anzidei et al. 2003b; Esposito et al., 2008). BA3D, BOTT, LINE, PNRL, PA3D

137 stations were established after the 2002 gas eruption while PANA station is part of the
138 Tyrrhenian Geodetic Network (Anzidei et al., 1995) and LIBI and PCOR of the IGMI network
139 (Surace, 1993). Only PANA station, which is located ~3 km west of the degassing zone, was
140 repeatedly occupied during five distinct campaigns before 2002 (Figures 2 and 3). So far most
141 of the GPS data were collected within the 2002-2006 time span (Table 1), after the gas
142 eruption. After the 2004 campaign, PANA was replaced by PA3D, located on the same
143 building at a distance of ~3 m.

144 The two continuous stations were installed at Panarea Island (CPAN) and at Lisca Bianca Islet
145 (LI3D) (Figure 2) on May 2004 and they are included in the RING network (Selvaggi et al.,
146 2006).

147 The non-continuous stations of Panarea network was repeatedly measured every six months in
148 the 2002-2006 time span using observation windows of 48-120 hour periods in each campaign
149 (Table 1).

150 We analyzed the GPS data set (1995-2007) of the Panarea network together with some
151 southern Italian and European EUREF permanent sites using the Bernese GPS software v.5.0
152 (Dach et al., 2007).

153 Daily loosely constrained solutions were generated for each campaign and later combined
154 with ~ 10 years of loosely constrained solutions of a regional network of continuous stations
155 in Italy, and surrounding regions, provided routinely by the INGV (Serpelloni et al., 2007). To
156 assure a reliable combination, nine continuous anchor IGS sites (Figure 2a) were always
157 included in all daily solutions. To express the time series in a stable reference frame, the
158 Panarea solutions were combined with other available clusters whose networks cover a large
159 part of the European region (Serpelloni et al., 2007). This strategy allowed us to obtain a daily
160 Helmert transformation on the ITRF2005 reference system (Altamimi et al., 2007), based on

161 20 common sites. The combined daily solutions were then transformed into the ITRF2005
162 reference system by estimating four parameters: three translations and a scale factor .
163 Fitting the ITRF2005 time series we estimated site velocities together with periodic signals,
164 eventual steps, always using the complete covariance matrix. To properly calibrate the formal
165 errors, the standard errors were re-scaled, according to the procedure proposed by Williams
166 (2003).

167 The velocity field with respect to the fixed Eurasian plate (Table 2) suggests a complex
168 kinematic framework, where regional tectonics and local volcanic and tectonic deformations
169 coexist. Comparing the residual velocity field relative to the Panarea network barycenter
170 (Panarea reference frame) with the one computed with respect to the Calabrian rigid block
171 (Gvirtzman and Nur, 1999, 2001; Doglioni et al.1991, D'Agostino and Selvaggi, 2004),
172 defined by the GPS sites PORO, CELL, VLSG and MSRU, did not reveal any significant
173 difference (0.39 ± 0.25 mm/yr) in the deformation field of Panarea. We therefore, concluded
174 that adopting the Panarea reference frame would allow to describe the local magmatic and
175 tectonic deformation from the regional deformation.

176

177 **Velocity and strain rate fields**

178 The GPS time series shown in Figure 3 are relative to the fixed Eurasian plate. A general
179 subsiding trend affects all the stations of the Panarea network with values ranging from -3 to -
180 9 mm/yr, with the exception of PCOR station. The latter is placed on the west sector of
181 Panarea Island and does not show any vertical motion.

182 PANA is the only GPS station observed before 2002 (Figure 3a), hence we used its data to test
183 the possibility of a change in the subsidence rate caused by the gas eruption. After November
184 2002, PANA was occupied during three different campaigns in December 2002, May 2003

185 and May 2004. Our analysis does not reveal any significant change in the rate of the Up
186 component of PANA, before and after the 2002 gas eruption (-6.7 ± 1.3 mm/yr before
187 November 2002; -7.4 ± 0.9 mm/yr after November 2002). A relevant feature recorded in the
188 PANA time series, a 4.2 ± 0.1 cm uplift, occurred between June 2000 and November 2002,
189 probably during the 2002 gas eruption.

190 Another puzzling discontinuity occurred at LI3D continuous station, located on Lisca Bianca
191 Islet (Figure 3b). Between June 18th and 19th 2005 an instantaneous step in the horizontal
192 components, of 12.1 ± 0.7 mm in the SE direction, was recorded. The inspection of this site
193 did not reveal any manipulation or failure of the receiver-antenna equipment and the GPS data
194 were continuously recorded during the event. Neither did the sky plot (i.e. the intrinsic noise
195 of each single GPS satellite range observation) reveal any anomaly during the entire month of
196 June 2005. For these reasons we argue that the signal recorded by LI3D is related to volcano
197 dynamics. In the same time the other continuous station, CPAN, not recorded a the horizontal
198 displacement indicate by an offset in time serie (Figure 3b)

199

200 The velocity field of the Panarea volcano with respect to the Panarea reference frame is shown
201 in Figure 2. PANA is the only site that was measured before the 2002 gas eruption and where
202 the pre- and post- event velocity can be estimated. Before the gas eruption its velocity was low
203 (1.8 ± 1.3 mm/yr) and WNW trending. Just after the gas eruption, it changed abruptly in
204 direction and magnitude, pointing towards SSE.

205 The horizontal velocity field, within the 2002 – 2007 time span, subdivides the Panarea area
206 into two different parts, which are separated by a major NE-trending fault system revealed by
207 bathymetric surveys (Gabbianelli et al., 1990; Gamberi et al., 1997; Anzidei et al., 2005). We
208 labeled “Area A” the one corresponding to the NW portion of Panarea Island and “Area B”

209 the one corresponding to the Islets area and the SE portion of Panarea Island (Figure 2). The
210 velocities of Area B are roughly convergent towards the 2002-2003 degassing area.
211 The horizontal strain rate estimated by STRAINGPS software (Pietrantonio and Riguzzi,
212 2004) of Area B, is shown in Figure 2b. The current deformation of the Islets area shows
213 contraction at 3.7 ± 0.5 μ strain/yr with a WNW trend.

214

215 4. Modeling of GPS data

216 Esposito et al. (2006) interpreted the 2002 gas eruption in terms of an accumulation at depth
217 of pressurized gas from a steady or quasi-steady release of gas from a deep magmatic source,
218 probably a cooling magma body, and from the periodic release of the overpressure when the
219 tensile strength of the overlying rocks is overcome either by the increased internal pressure or
220 by external changes in the tectonic stress.

221 Starting with this qualitative model of Panarea volcano we analytically modeled the GPS
222 results collected between 2002, after the November crisis, and 2007.

223 We defined the computational domain of Panarea volcano (Figure 4) as composed of a largely
224 submarine volcano extended below sea level for 1100 m and of emerged islands above sea
225 level characterized by the presence of a hydrothermal-geothermal system where volcanic gas
226 sampled in 2002-2003 had an estimated temperature of up to 300°C and a bulk fluid pressure
227 of about 100 bar (Chiodini et al., 2006). We also considered the presence of a) a regional NE-
228 SW fault system as suggested by structural data (Gamberi et al., 1997; De Astis et al., 2003;
229 Esposito et al., 2006; Esposito, 2007; Acocella et al., 2008) and constrained by GPS results; b)
230 two main vertical fracture systems with NNE and NW trends located west of Bottaro Islet that
231 have been the main pathways for upwelling of hydrothermal fluids (Esposito et al., 2006).

232 We exploited the capability of the Okada solutions (Okada, 1985) to model the GPS data.
233 Although such models account for only an elastic behavior, neglecting heterogeneities and
234 structural discontinuities, they are widely used in the modeling of volcanic areas (Dvorak and
235 Dzurisin, 1997; Miura et al., 2000; Lowry et al., 2001; Jousset et al., 2003; Lagios et al., 2005;
236 Sepe et al., 2006) where cracks or discontinuities slightly alter the elastic constants but not the
237 fundamental elastic behavior of a volcano (Jaeger and Cook, 1977; Dvorak and Dzurisin,
238 1997).

239 To reproduce the realistic hydrothermal-geothermal system (Figure 4), we carefully set up a
240 system of four tensile/shear sources, partially constrained (see Table 3) by the geochemical,
241 volcanological and structural remarks illustrated above.

242 The depth of the pressure source is assessed to be between 800 m and 900 m accounting for
243 the geochemical data (Chiodini et al., 2006). The NE major regional fault system, dipping 70°
244 with an azimuth of 45° from the north (Gamberi et al. 1997; De Astis et al., 2003; Esposito,
245 2007; Acocella et al., 2008), is considered to have an infinite length to avoid the unrealistic
246 border effects; finally, the two vertical fracture systems, NNE (27°) and NW (135°) located at
247 Islets area, are modeled with two segments of length 1100 m and 800 m, respectively
248 (Esposito et al., 2006).

249 For the retrieval of the source parameters left free (Table 3), we used a non-linear inversion
250 algorithm based on the Levenberg-Marquardt least-square approach (Levenberg, 1944;
251 Marquardt, 1963) and its implementation in the MINPACK library (Moré et al, 1980). This
252 algorithm is an efficient combination of the gradient descent and the Gauss-Newton
253 algorithms (Press et al., 1992) and the best-fit configuration of the parameter vector \mathbf{m} is
254 found by minimization of a cost function of the type:

255
$$\chi^2(\mathbf{m}) = \sum_i^N \left[\frac{d_{i,obs} - d_{i,mod}(\mathbf{m})}{\sigma_i} \right]^2$$

256 where, for the i^{th} point, d_{obs} are the observed data, $d_{mod}(\mathbf{m})$ are the predicted data based on the
 257 model \mathbf{m} and σ_i are the standard deviations coming from the GPS data processing.

258 Our results (Table3) show that the source that best fits the GPS velocities during post eruption
 259 stage is a composite by inflation/deflation of a hydrothermal /geothermal system combined
 260 with movement along the regional NE-SW fault and displacements of the fracture systems at
 261 the 2002 degassing area.

262 The model results show (italic in Table 3) the horizontal source located at a depth of 900 m
 263 and characterized by a vertical movement of -0.7 cm/yr. The NE regional fault, 800 m wide,
 264 shows a rake of -120°, 0.2 cm/yr of slip and an opening of 0.3 cm/yr. The NW fracture
 265 system is 800 m wide with a negligible displacement while the NNE fracture system, 900 m
 266 wide, shows a closing of -0.7 cm/yr. Results show good reliability: the RMS of the residual
 267 of the best-fit solution is 0.2 cm/yr and the normalized χ^2 is 1.1. Figure 2 shows the velocity
 268 field obtained by GPS data and the results of the inversion .

269 In addition, we tried to test the reliability of a Mogi (1958) point-pressure source, setting this
 270 source beneath the Islets area. Unfortunately, this simple model could not explain the
 271 displacements of the Panarea GPS network, because of the wide discrepancy between the
 272 observed and the modeled data ($\chi^2 = 3.12$), and was therefore, excluded.

273

274 **5. Discussion**

275 Gas eruptions are typical of active volcanoes as a consequence of the combination of several
 276 processes that may involve only the variations of pressure and temperature conditions in
 277 hydrothermal/geothermal systems and/or the response to shallow magmatic intrusions

278 (Battaglia et al., 2006; Gottsmann et al., 2007). The 2002 gas eruption at Panarea volcano
279 reflects a deep magmatic intrusion which modified the equilibrium of the
280 hydrothermal/geothermal system reservoir (Chiodini et al., 2006; Capaccioni et al., 2007).
281 We propose a sketch to explain the evolution of the 2002 gas eruption using GPS velocities
282 compared to the volcanological and structural framework. The sketch defines three stages *pre-*
283 *, syn-* and *post-*gas eruption (Figure 5). The hydrothermal/geothermal system is represented by
284 two layers: a) a fluid reservoir b) a shallow reservoir characterized by a mixture of volcanic
285 fluids and marine water. We consider that Area A, including the NW portion of Panarea
286 Island, is mostly made of coherent rocks, whereas Area B, representing the SE portion of
287 Panarea Island and the Islets, is characterized by highly fractured and permeable rocks.

288

289 ***Pre-eruption stage – Stage 1***

290 In the *pre-eruption* stage the PANA GPS site recorded a subsidence of 6.7 ± 1.3 mm/yr
291 (Figure 3) with a WNW motion of about 2 mm/yr (Figure 2). During this period degassing
292 was mild and mostly located in Area B (Islets area) and, subordinately, in Panarea Island (La
293 Calcara, Figures 1 and 4) and Basiluzzo (Punta Levante, Figures 1 and 4). In stage 1,
294 conditions for degassing depend on the rock properties. Hydrothermal fluids upwell mostly
295 through the highly fractured rock mainly present in Area B, without overpressure since
296 fractures are semi-opened. The gas pressure inside the reservoir (Figures 4 and 5) is P_1 and
297 the tensile strengths of rocks are τ_A and τ_B in correspondence of Area A and Area B,
298 respectively. We assumed $\tau_B < \tau_A$, since Area B is characterized by more intense fracturing. P_1
299 does not reach the tensile strengths of the rocks.

300 ***Syn-eruption stage - Stage 2***

301 The addition of magmatic gases in 2002 (Caliro et al., 2004; Capaccioni et al., 2007) within
302 the hydrothermal/geothermal system induced an increase of pressure and temperature and
303 produced the gas eruption in the Islets area (Area B), with the opening of hundreds of gas
304 vents aligned NNE and NW trending (Anzidei et al., 2005; Esposito et al., 2006) and vertical
305 crustal deformation of 4.2 ± 0.1 cm recorded at PANA site, located at ~ 3 km to the west, in
306 Area A. Furthermore, about 20 low magnitude ($M_d \geq 1.0$) and high-frequency seismic events
307 occurred on November 3, 2002 between 3:37 GMT and 5:00 GMT i.e. only a few hours
308 before the local inhabitants of Panarea witnessed boiling sea in the surroundings of Lisca
309 Bianca and Bottaro (Saccorotti et al., 2003; Linde et al., 1994). Stage 2 is characterized by an
310 increase in pressure inside the horizontally extended reservoir, where $P_2 \gg P_1$, favors
311 conditions for the initiation of hydrofractures and rupture. This condition is expressed by the
312 relation $p_l + p_e \geq \sigma_3 + \tau$ (Gudmundsson et al., 2001) where p_l is the lithostatic pressure,
313 p_e is the exceeding pressure obtained by the difference between pressure P_2 , in the reservoir
314 at the time of the rupture and the lithostatic pressure, σ_3 is the minimum compressive
315 (considered positive) principal stress, acting perpendicular to the fractures and τ is the tensile
316 strength of the rocks (τ_A and τ_B at Area A and Area B, respectively). Normally, rupture and
317 initiation of hydrofractures occur when p_e reaches the tensile strength of the local rocks
318 (Gudmundsson et al., 2001).

319 ***Post-eruption stage - Stage 3***

320 GPS data collected after the gas eruptive event in the 2002 - 2007 time span, (Figure 3) show
321 a general subsidence with a mean rate from -3 to -9 mm/yr. This subsidence is likely to be
322 associated with degassing of the hydrothermal/geothermal system, though a rate of subsidence
323 spread over the region of the Aeolian Islands is present (Bonaccorso, 2002; Mattia et al.,

324 2008). The planar velocities of Area B are roughly convergent towards the 2002 degassing
325 area (Figure 2). The pre-eruption conditions, in terms of flux intensity and geochemical
326 characters, were restored in a relatively short time as suggested by Capaccioni et al. (2007).
327 Gas pressure decreased ($P_3 \ll P_2$) and the degassing became located only along the principal
328 locations of vents opened during the gas eruption within Area B.

329 Post-eruptive conditions may also involve the discharge of hydrothermal fluids through
330 opened fractures at Area B causing a progressive closure of some fractures by self-sealing
331 processes induced by the progressive drop of pressure and temperature (Gudmundsson 1999,
332 2001; Olsen et al., 1998; Cas et al., 2009) and changing the intrinsic value τ of the tensile
333 strength of the rocks.

334 Continuous GPS data collected at the Islets area have also shown a clear and very rapid
335 deformation with horizontal, but not vertical, displacements at the Lisca Bianca site (Figure
336 3).

337 According to the results of the Okada model (Table 3) the decrease in fluid pressure ΔP that
338 occurred passing from Stage 2 to Stage 3, can be determined by using the relation
339 (Gudmundsson, 1999)

$$340 \quad \Delta P = \frac{\Delta W \cdot E}{2L(1 - \nu^2)}$$

341 where ΔW is the modeled displacement, E is Young's modulus of the rocks in Area B, L is
342 the length of the modeled faults and ν is Poisson's ratio of the rocks.

343 Assuming that the static Young's modulus of the basaltic-dacite outcropping in Area B is
344 $E=15$ GPa , $\nu=0.25$ (Gudmundsson, 1999; Schultz, 1995), and ΔW and L are given by the
345 Okada modeling (Table 3), we obtain a decreased fluid pressure of 0.05 MPa for the NNE
346 system and negligible variations for the NW source.

347 This rough estimate of the pressure suggests that the present-day degassing of the Panarea
348 hydrothermal/geothermal system is mainly controlled by the NW faults system present in
349 Area B. At any rate, the effects of pressure and temperature changes within the
350 hydrothermal/geothermal fluids, are distributed throughout Panarea volcano, as shown by the
351 subsidence trend and by the horizontally extended reservoir model (Table 2 and Figures 2 and
352 5).

353

354 The scenario proposed by the modeling of post-eruption stage deformations is consistent with
355 GPS pattern velocities and with tectonic and volcanic data. Velocity patterns can generally be
356 interpreted in terms of simple source geometries that represent sills, dikes or plugs. The
357 migration of hot fluid inside the hydrothermal/ geothermal system plays a role to magnitude
358 and geometry of ground surface displacements in volcanic systems (e.g. Todesco et al., 2003,
359 2004; Battaglia et al., 2006; Hurwits et al., 2007).

360 Our model results point out the role of NE- and NW- trending fractures as the main pathways
361 for the gas exhalation in the Islets area and identify the crucial role of the regional
362 discontinuity NE-SW located between Panarea island and Islets area (Gamberi et al., 1997; De
363 Astis et al., 2003; Esposito et al., 2006; Esposito, 2007; Acocella et al., 2008). The November
364 2002 gas eruption can be interpreted as the evolution of a hydrothermal system fed by a deep
365 source of magmatic fluids capable to build up pressure and temperature at some shallow level
366 where the migration of fluids causes periodically the tensional strength of the confining rocks
367 to be overcome allowing the sudden release of the pressurised gas

368 The relationship between earthquake and volcano eruption was revealed by certain statistical
369 analysis of events of global scale (Newhall and Dzurisin, 1988; Linde and Sacks, 1998). In

370 events with $M_l \geq 8$ the seismic wave produced by the earthquake may disturbs: a) the magma
371 reservoir, leading to eruption b) the status of the regional stress by changing it.

372 The November 3, 2002 gas eruption followed the earthquake (M_l 5.6) of September 6th
373 between Palermo and Ustica Island, correlating with several aftershocks, the strongest of
374 which of M_l 4.3 (Azzaro et al., 2004, Rovelli et al., 2004) and with the onset of the strong
375 eruption at Mt Etna on October 27th. It preceded the paroxysmal eruption at Stromboli that
376 began December 28th and finished with an explosion on April 5, 2003. The Palermo
377 earthquake changed the regional strain and triggered the reservoirs of three volcanoes (Walter
378 et al., 2009). The eastern portion of the Aeolian Islands is characterized by an extensional
379 regional strain consistent with a greater vulnerability to the dynamic triggering (Hill, 2008). A
380 similar sequence of events occurred in the Southern Tyrrhenian area in 1865 (Esposito et al.,
381 2006; Billi and Funicello, 2008) as reported by Mercalli (1883).

382

383 **6. Conclusion**

384 The implementation and monitoring of the Panarea local GPS network have allowed to define
385 a detailed pattern of deformation, unknown before the 2002 gas eruption. Results from the
386 local GPS network are mainly sensitive to the local deformation field rather than the
387 extensional regional deformation field recognized in the eastern sector of the Aeolian Islands.

388 Two different kinematic domains have been recognized in the Panarea area, separated by the
389 regional NE-SW fault: Area A, which includes NW portion of Panarea Island, and Area B
390 which includes the Islets area and SE portion of Panarea Island. In the Islets area, a shortening
391 WNW-trend in the order of 10^{-6} yr^{-1} , has been estimated within the 2002-2007 time span. GPS
392 results (2002-2007) have been modeled by an elastic, homogenous, isotropic half-space
393 system strongly influenced and related to hydrothermal/geothermal fluid migration. The best-

394 fitting model for GPS data collected at post eruption stage, was found through a combination
395 of Okada sources. One wide and horizontally extended reservoir simulates the source of
396 pressure within the hydrothermal/geothermal system, at a depth of ~ 900 m. The upwelling of
397 gas along the NNE- and NW trending fractures at Islets area on 2002-2003 was favored by
398 tectonic setting and the mechanical property of rocks. The present day WNW shortening is
399 consistent with closing along NNE fractures, as suggested by the Okada model. The
400 overpressure data suggests that, presently, the degassing of the Panarea
401 hydrothermal/geothermal system is mainly controlled by NW fracture systems.

402 We also believe that the continuous and general subsidence trend observed, during the 1995 –
403 2007 time span, is mainly due to a decrease of the thermo-baric conditions within the
404 hydrothermal/geothermal system although also a subsidence in the region of the Aeolian
405 Islands is recognized (Bonaccorso, 2002; Mattia et al., 2008).

406 The November 3, 2002 degassing was triggered by changes in the extensional regional strain
407 oriented NW-SE in the eastern Aeolian arc. Modeling of GPS data also provides new
408 indications on the regional NE-SW fault system, that has an oblique kinematics, suggesting an
409 additional component of dextral shear and a predominantly NW-SE normal extension
410 observed by structural data. The extension value estimated by the model (0.3 cm/yrs) is
411 consistent with the value <100 nanostrain/yr (D'Agostino and Selvaggi, 2004, Esposito, 2007)
412 recognized in the eastern Aeolian arc.

413 The continuous GPS data recording on the Islets area has allowed to monitor the evolution of
414 the degassing phases, evidencing that horizontal quasi-instantaneous displacement occurred
415 on June 2005 at Lisca Bianca Islet. Such displacement is characterized by aseismic spreading
416 and/or cracks closure while vertical displacement has not been recorded. This sudden offset is
417 recorded only at LI3D continuous station. We suppose that it may be connected to a very local

418 fracture system rather than a signal of broader tectonic origin, probably due to migration of
419 pressurised fluids that exert an additional pore-pressure over country rocks..

420

421 The GPS Panarea network is a powerful tool to understand the ground deformations at a local
422 scale, in the short and long-term, due to fluid migration in the hydrothermal/geothermal
423 systems.

424 Therefore, the Panarea volcano deserves the same monitoring and hazard assessment effort of
425 any active volcano located nearby human settlements. In particular, the most critical scenario,
426 of the potential hazard, is related to phreatic eruptions that may occur offshore as well as on
427 the inhabited island of Panarea.

428

429 **Acknowledgments**

430 Funding of this research came from the Italian Civil Protection Agency. We thank Nicolas
431 Fournier for the constructive comments to improve the manuscript.

432

433 **References**

434 Acocella, V., Neri, M., Walter, T. (2008) Structural features of Panarea volcano in the frame of
435 the Aeolian Arc (Italy): implications for the 2002–2003 unrest, *Journal of Geodynamics*
436 doi:10.1016/j.jog.2009.01.004

437

438 Altamimi, Z., X. Collilieux, J. Legrand, B. Garayt and C. Boucher (2007), ITRF2005: A new
439 release of the International Terrestrial Reference Frame based on time series of station
440 positions and Earth Orientation Parameters, *J. Geophys. Res.*, 112, B09401,
441 Doi:10.1029/2007jb004949, 2007

442 Anzidei, M., P. Baldi, G. Casula, F. Riguzzi, L. Surace (1995), La rete Tyrgeonet, Suppl. Bol.
443 geod. e scien. aff., Suppl. Bol. geod. e scien. aff., Istituto Geografico Militare Italiano, Vol.
444 LIV, n.2.
445

446 Anzidei, M. (2000), Rapid bathymetric surveys in marine volcano areas: a case study in
447 Panarea area, Phys. Chem. Earth (a), 25, No.1, pp. 77-80.
448

449 Anzidei, M. and A. Esposito (2003a), New insights from resolution bathymetric surveys in the
450 Panarea volcanic Complex, Geophys. Res. Abstr. 5, 05923 EGS, Nizza
451 <http://www.cosis.net/abstracts/EAE03/05923/EAE03-J-05923.pdf>
452

453 Anzidei, M., A. Esposito, E. Serpelloni, P. Baldi, A. Benini and G. Giordano (2003b), GPS
454 and bathymetric surveys in the Panarea volcanic complex (Aeolian Island, Italy), GNV
455 General Assembly, Roma, June 9-11.

456 Anzidei, M., A. Esposito, G. Bortoluzzi and F. De Giosa (2005), The high resolution
457 bathymetric map of the exhalative area of Panarea Aeolian islands, Italy. Ann. of Geophys.,
458 48, n.6, pp. 899-921
459

460 Anzidei, M., P. Baldi, Fabris M., (2006), integrazione di dati fotogrammetrici, LIDAR e
461 batimetrici nell' arcipelago delle isole Eolie, Bollettino della Società Italiana di
462 Fotogrammetria e Topografia, n.1, 13-26.
463

464 Azzaro R., M.S. Barbano, R. Camassi, S. D'Amico, A. Mostaccio, G. Piangiamore and L.
465 Scarfi (2004), The earthquake of 6 September 2002 and the seismic history of Palermo

466 (Northern Sicily, Italy): Implications for the seismic hazard assessment of the city. *J. of*
467 *Seismology* 8, 525–543.

468

469 Barberi, F., P. Gasparini, F. Innocenti and L. Villari (1973), Volcanism of the Southern
470 Tyrrhenian sea and its geodynamic implications. *J. Geophys. Res.* 78, 5221-5232.

471

472 Battaglia, M., C. Troise, F. Obrizzo, F. Pingue, and G. De Natale (2006), Evidence for fluid
473 migration as the source of deformation at Campi Flegrei caldera (Italy), *Geophys. Res. Lett.*,
474 33, L01307, doi:10.1029/2005GL024904.

475

476 Beccaluva, L., G. Gabbianelli, F. Lucchini. L. Rossi and C. Savelli (1985), Petrology and
477 K/Ar ages of volcanic dredged from the Aeolian seamounts: implications for geodynamic
478 eruption of the southern Tyrrhenian basin, *Earth Planet. Sci. Lett.* 74, 187-208.

479

480 Bellia, S., M. L. Carapezza, F. Italiano and P. N. Nuccio (1986), Caratteristiche delle
481 emissioni geotermiche sottomarine ad Est di Panarea (Isole Eolie), *Proceedings of the V*
482 *Italian Conference, GNGTS*, 1191-1202.

483

484 Bellia, S., F. Italiano and P. N. Nuccio (1987), Le strutture sommerse ad est di Panarea Isole
485 Eolie: definizione di una loro natura antropica sulla base di studi mineralogici, petrografici e
486 geochimici. I.G.F. C.N.R. Palermo, 3.

487

488 Billi, A. and Funicello, R. (2008), Concurrent eruptions at Etna, Stromboli, and Vulcano:
489 casualty or causality?: *Annales de Geophysique*, v. 51, 655-725

490 Bonaccorso, A. (2002), Ground deformation of the southern sector of the Aeolian Islands
491 volcanic arc from geodetic data, *Tectonophysics*. 351,181–192.
492

493 Calanchi, N., B. Capaccioni, M. Martini, F. Tassi, and L. Valentini (1995), Submarine gas-
494 emission from Panarea Island Aeolian Archipelago: distribution of inorganic and organic
495 compounds and inferences about source conditions, *Acta Vulcanologica* 7, 1, 43-48.
496

497 Calanchi, N., C. A. Tranne, F. Lucchini, P.L. Rossi and I.M. Villa (1999), Explanatory notes
498 to the geological map (1:10.000) of Panarea and Basiluzzo islands (Aeolian arc. Italy), *Acta*
499 *Vulcanologica*, 11, 2, 223-243.
500

501 Caliro, S., A. Caracausi, G. Chiodini, M. Ditta, F. Italiano, M. Longo, C. Minopoli, P.M.
502 Nuccio, A. Paonita and A. Rizzo (2004), Evidence of a new magmatic input to the quiescent
503 volcanic edifice of Panarea, Aeolian Islands, Italy. *Geophys. Res. Lett.* 31, L07619,
504 doi:10.1029/2003GL019359.
505

506 Capaccioni, B., F. Tassi, D. Vaselli, D. Tedesco, and P. M. L. Rossi. (2005), The November
507 2002 degassing event at Panarea Island (Italy): The results of a 5 months geochemical
508 monitoring program, *Ann. Geophys.*, 48, 755– 765.
509

510 Capaccioni, B., F. Tassi, D. Vaselli, D. Tedesco, and Poreda R. (2007), Submarine gas burst at
511 Panarea Island (Southern Italy) on 3 November 2002: A magmatic versus hydrothermal
512 episode. *J. Geophys. Res.* 112, B05201, Doi:10.1029/2006jb004359.
513

514 Cas, R., G. Giordano, A. Esposito and F. Balsamo (2007), Hydrothermal breccia textures and
515 processes: Lisca Bianca Islet, Panarea, Aeolian Islands, Italy. Breccia Symposium – Economic
516 Geology Res. Unit, James Cook University, Townsville, Australia.
517

518 Cas, R., G. Giordano, A. Esposito and F. Balsamo (2009), Hydrothermal breccia textures and
519 processes: Lisca Bianca Islet, Panarea, Eolian Islands, Italy. Symposium – Economic Geology
520 Res.(submitted).
521

522 Chiodini, G., S. Caliro, G. Caramanna, D. Granirei, C. Monopoli, R. Moretti, L. Perotta and
523 Ventura G. (2006), Geochemistry of submarine gaseous emission of Panarea Aeolian Islands,
524 Southern Italy: Magmatic vs. Hydrothermal origin and implications for volcanic surveillance,
525 Pure appl. Geophys. 163, 759-780 0033-4553/06/040759-22 DOI 10.1007/s00024-006-0037-
526 y.
527

528 Cocchi, L., F. Caratori Tontini, C. Carmisciano, P. Stefanelli, M. Anzidei, A. Esposito, C. Del
529 Negro, F. Greco and R. Napoli (2008), Looking inside the Panarea Island (Aeolian
530 Archipelago, Italy) by gravity and magnetic data. Ann. Geophys. 55, 25-38
531

532 Dach, R., Hugentobler U.,Fridez P.and Meindl M. (2007), Bernese GPS software version 5.0
533 AIUB
534

535 D'Agostino, N. and G. Selvaggi (2004), Crustal motion along the Eurasia-Nubia plate-
536 boundary in the Calabrian Arc and Sicily and active extension in the Messina Straits from
537 GPS measurements, J. Geophys. Res., 109, B11402, doi: 10.1029/2004 JB002998

538 De Astis, G., G. Ventura G and G. Vilardo (2003), Geodynamic significance of the Aeolian
539 volcanism (Southern Tyrrhenian Sea, Italy) in light of structural, seismological and
540 geochemical data. *Tectonics* .22, 4, 1040, doi:10.1029/2003TC001506.
541

542 Doglioni, C., Innocenti F. and Mariotti G., 2001. Why Mt Etna?, *Terra Nova*, 13, 25–31.
543

544 Dolfi, D., D. de Rita, C. Cimarelli, S. Mollo, M. Soligo, M, Fabbri (2006), Dome growth
545 rates, eruption frequency and assessment of volcanic hazard: Insights from new U/Th dating
546 of the Panarea and Basiluzzo dome lavas and pyroclastics, Aeolian Islands, Italy. *Quaternary*
547 *Int.* 162–163, 182–194
548

549 Dvorak, J. and Dzurisen D. (1997), *Volcano Geodesy: The Search For Magma Reservoirs*
550 *And The Formation Of Eruptive Vents.* *Rev. Geophys.*, 35, 3, 343–384.

551 Esposito A., G. Giordano and M. Anzidei (2006), The 2002–2003 submarine gas eruption at
552 Panarea volcano Aeolian Islands, Italy: volcanology of the seafloor and implications for the
553 hazard scenario, *Marine Geology* 227, 119–134.
554

555 Esposito A. (2007), *Studio della deformazione geodetica delle Isole Eolie con particolare*
556 *referimento al vulcano di Panarea.* PhD Thesis Università di Bologna (Italy)
557

558 Esposito A., M., Anzidei, A. Pesci, G. Pietrantonio and G. Giordano (2008), Evidence of
559 active deformation of the Panarea volcano (Aeolian Island, Italy) from GPS data. *J. Volcanol.*
560 *Geotherm. Res. Special Issue "Reducing volcanic Risk in Islands, in press*
561

562 Faccenna C., T. W. Becker, F. P. Lucente, L. Jolivet and F. Rossetti (2001), History of
563 subduction and back-arc extension in the central Mediterranean, *Geophys. J. Int.*, 145, 809–
564 820.

565

566 Favalli M., D. Kartson, R. Mazzuoli, M. T. Pareschi and G. Ventura (2005), Volcanic
567 geomorphology and tectonics of the Aeolian archipelago Southern Italy based on integrated
568 DEM data, *Bull Volcanol.* 68, 157-170.

569

570 Gabbianelli G., P.Y. Gillot, G. Lanzafame, C. Romagnoli and P. L. Rossi (1990), Tectonic
571 and volcanic evolution of Panarea (Aeolian Island, Italy), *Marine Geology*, 92, 312-326.

572

573 Gabbianelli G., C. Romagnoli, P. L. Rossi and N. Calanchi (1993), Marine Geology of
574 Panarea–Stromboli area. Aeolian Archipelago, Southeastern Tyrrhenian sea, *Acta Vulcanol.* 3,
575 11-20.

576

577 Gamberi F., P. M. Marani and C. Savelli (1997), Tectonic volcanic and hydrothermal features
578 of submarine portion of Aeolian arc (Tyrrhenian Sea), *Marine Geology* 140, 167-181.

579

580 Gottsmann J., R. Carniel, N. Coppo, L. Wooller, S. Hautmann and H. Rymer (2007)
581 Oscillations in hydrothermal systems as a source of periodic unrest at caldera volcanoes:
582 Multiparameter insights from Nisyros, Greece. *Geophys. Res. Lett.*, 34, L07307,
583 Doi:10.1029/2007gl029594

584

585 Gudmundsson A., (1999), Fluid overpressure and stress drop in fault zones. *Geophys. Res.*
586 *Lett.* 26, 115-118.
587
588 Gudmundsson A., S.S. Berg, K. B. Lyslo and E. Skurtveit (2001), Fracture networks and Fluid
589 transport in active fault zones. *J. Structural Geology* 23, 343-353
590
591 Gvirtzman Z. and A. Nur A (1999), The formation of Mount Etna as the consequence of slab
592 rollback, *Nature*, 401, 782–785.
593
594 Gvirtzman Z., and A. Nur (2001), Residual topography, lithospheric structure and sunken
595 slabs in the central Mediterranean, *Earth Planet. Sc. Lett.*, 187, 117-130.
596
597 Hill D.P. (2008), Dynamic stresses, coulomb failure, and remote triggering: *Bulletin of the*
598 *Seismological Society of America*, v. 98, p. 66–92, doi: 10.1785/0120070049.
599
600 Hollenstein C. H., H. G. Kahle, A. Geiger, S. Jenny, S. Goes and D. Giardini (2003), New
601 GPS constraints on the Africa-Eurasia plate boundary zone in southern Italy, *Geophys. Res.*
602 *Lett.*, 30, 18. 1935,doi:10.1029/2003GL017554.
603
604 Hurwitz S., L. B. Christiansen, and P. A. Hsieh (2007), Hydrothermal fluid flow and
605 deformation in large calderas: Inferences from numerical simulations, *J. Geophys. Res.*, 112,
606 B02206, doi:10.1029/2006JB004689.
607

608 Italiano F. and P. M. Nuccio (1991), Geochemical investigations of submarine volcanic
609 exhalations to the east Panarea, Aeolian Islands, Italy. *J. Volcanol. Geotherm. Res.*, 46, 125-
610 141.

611

612 Jousset P., Mori H and Okada H. (2003). Elastic models for the magma intrusion associated
613 with the 2000 eruption of Usu Volcano, Hokkaido, Japan. *J. Volcanol. Geotherm. Res.*, 125,
614 81-106.

615

616 Lagios E, V. Sakkas, I. Parcharidis and V. Dietrich (2005). Ground deformation of Nisyros
617 Volcano (Greece) for the period 1995–2002: Results from DInSAR and DGPS observations.
618 *Bull Volcanol* (2005) 68: 201–214 DOI 10.1007/s00445-005-0004-y

619

620 Levenberg K. (1944), A Method for the Solution of Certain Non-Linear Problems in Least
621 Squares, *The Quarterly of Applied Mathematics* 2, 164–168.

622

623 Linde A. T. and I. S. Sacks (1998), Triggering of volcanic eruptions, *Nature* 395, 888-890.

624

625 Linde, A. T., Sacks, I. S., Johnston, M. J. S., Hill, D. P. & Bilham, R. G.(1994) Increased
626 pressure from rising bubbles as a mechanism for remotely triggered seismicity. *Nature* 371,
627 408–410..

628

629 Lowry A.R., M.W. Hamburger, C.M. Meerten, E.and G. Ramo (2001). GPS monitoring of
630 crustal deformation at Taal Volcano,Philippines. *J. Volcanol. Geotherm. Res.*, 105, 35 - 47.

631

632 Lucchi F., C. A. Tranne, N. Calanchi, J. Keller and P. L. Rossi (2007), Geological map of
633 Panarea and minor islets (Aeolian Islands), University of Bologna, University of Freiburg and
634 INGV, L.A.C. Firenze.

635

636 Marquardt, D. (1963), An Algorithm for Least-Squares Estimation of Nonlinear Parameters,
637 SIAM, J. on Applied Mathematics 11, 431–441

638

639 Mattia M., M. Palano, V. Bruno, F. Cannavò, A. Bonaccorso and S. Gresta (2008), Tectonic
640 features of the Lipari–Vulcano complex (Aeolian archipelago, Italy) from 10 years (1996–
641 2006) of GPS data, *Terra Nova* 20, 5,, 370-377

642

643 Mercalli, 1883. *Vulcani e fenomeni Vulcanici*. In: Negri, G., Stoppani, A., Mercalli, G. Eds.
644 *Geologia d’Italia* 3rd part. Milano, 374 pp.

645

646 Miura S., Sadato Ueki, Toshiya Sato, Kenji Tachibana, and Hiroyuki Hamaguchi (2000).
647 Crustal deformation associated with the 1998 seismo-volcanic crisis of Iwate Volcano,
648 Northeastern Japan, as observed by a dense GPS network. *Earth Planets Space*, 52, 1003–
649 1008.

650

651 Mogi, K. (1958), Relations between eruptions of various volcanoes and the deformation of the
652 ground surface around them, *Bull. Earthquake Res. Inst. Univ. Tokyo*, 36, 99– 134.

653

654 Moré, J.J, B. S. Garbow and K. E. Hillstrom (1980), User Guide for MINPACK-1, Argonne
655 National Laboratory Report ANL-80-74.

656

657 Okada, Y. (1985), Surface deformation due to shear and tensile faults in a half-space, Bull.
658 Seism. Soc. Am., 75, 1135-1154.

659

660 Olsen M. P. and C. Scholz (1998), Healing and sealing of a simulated fault gouge under
661 hydrothermal conditions: Implications for fault healing. J. Geophys. Res., 103, No. B4, Pages
662 7421-7430, April 10, 1998

663

664 Pietrantonio G. and F. Riguzzi (2004), Tree-dimensional strain tensor estimation by GPS
665 observations: methodological aspects and geophysical applications, J. Geodynamic 38, 1-18.

666

667 Pondrelli, S., C. Piromallo, and E. Serpelloni, (2004), Convergence vs. retreat in Southern
668 Tyrrhenian Sea: Insights from kinematics, Geophys. Res. Lett., 31, L06611,
669 doi:10.1029/2003GL019223.

670

671 Press, W.H., S. Teukolsky, W. T. Vetterling and B.P. Flannery, (1992), Numerical recipes in
672 C, Cambridge University Press, Cambridge, 1992

673

674 Romano R. (1973), Le isole di Panarea e Basiluzzo. Riv. Miner. Siciliana 139-141, pp. 49-86.

675

676 Rovelli A., Vuan, A., Mele, G., Priolo, E., and Boschi , E., 2004, Rarely observed shortperiod
677 (5–10 s) suboceanic Rayleigh waves propagating across the Tyrrhenian Sea: Geophysical
678 Research Letters, v. 31, L22605, doi:10.1029/2004GL021194.

679

680 Saccorotti, G., D. Galluzzo, M. La Rocca, E. Del Pezzo. and D. Patanè (2004), Attività
681 sismica registrata a Panarea. In “Convenzione DPC-INGV per lo studio e il monitoraggio
682 dello Stromboli e Panarea”. Istituto Nazionale di Geofisica e Vulcanologia, Repertorio n.427
683 del 20.6.2003. Relazione sull’attività 2003.

684

685 Selvaggi, G., A. Avallone, N. D' Agostino, L. Abruzzese, M. Anzidei, M. Cantarero, V.
686 Cardinale, A. Castagnozzi, G. Casula, G. Cecere, R. Cogliano, F. Criscuoli, C. D' Ambrosio,
687 E. D' Anastasio, P. De Martino, S. Del Mese, G. De Luca, R. Devoti, L. Falco, V. Flammia,
688 A. Galvani, L. Giovani, I. Hunstrad, A. Massucci, M. Mattia, A. Memmolo, F. Migliari, F.
689 Minichiello, R. Moschillo, F. Obrizzo, M. Palano, G. Pietrantonio, M. Pignone, M. Pulvirenti,
690 M. Rossi, F. Riguzzi, E. Serpelloni, U. Tammaro, L. Zarrilli (2006), La "Rete Integrata
691 Nazionale GPS" (RING) dell’INGV: una infrastruttura aperta per la ricerca scientifica.
692 Proceedings ASITA, 10, 1749-1754. <http://ring.gm.ingv.it/>

693

694 Sepe V., Atzori S. and Ventura G. (2007). Subsidence due to crack closure and
695 depressurization of hydrothermal systems: a case study from Mt Epomeo (Ischia Island, Italy)
696 Terra Nova, 00, 1–6, 2007 doi: 10.1111/j.1365-3121.2006.00727.

697

698 Serpelloni E., M. Anzidei, P. Baldi, G. Casula, A. Galvani, A. Pesci and F. Riguzzi, (2002),
699 Combination of permanent and non-permanent GPS networks for the evaluation of the strain-
700 rate field in the central Mediterranean area, Boll. Geofis. Teor. Appl., 43, 195-219.

701

702 Serpelloni E, A. Cavaliere, G. Pietrantonio, A. Galvani, A. Esposito, V. Sepe, R. Devoti and
703 F. Riguzzi F (2007), Data Analysis of Permanent GPS Sites (RING) Italy, Eos Trans. AGU,
704 Fall Meeting 2007, Abstract G21C-0659.

705

706 Schultz R.A., (1995), Limits on strength and deformation properties of jointed basaltic rock
707 masses. *Rock Mechanics and Rock Engineering* 28, 1±15.

708

709 Surace L., (1993), Il progetto IGM95, *Boll. Geodesia e Scienze Affini*, 3, 220-230

710

711 Tallarico A., M. Dragoni, M. Anzidei and A. Esposito (2003), Modeling long-term round
712 deformation due to the cooling of a magma chamber: case of Basiluzzo island, Aeolian
713 islands, Italy. *J. Geophys. Res.*, . 108, No B 12, 2568, 10.1029/2002 JB002376.

714

715 Tikku A. A., D. C McAdoo., M. S. Schenewerk. and E. C. Willoughby (2006), Temporal
716 fluctuations of microseismic noise in Yellowstone’s Upper Geyser Basin from a continuous
717 gravity observation. *Geophys. Res. Lett.* 33, L11306, Doi:10.1029/2006gl026113.

718

719 Tizzani P., M. Battaglia, G. Zeni, S. Atzori, P. Berardino, R. Lanari (2009). Uplift and Magma
720 Intrusion at Long Valley caldera from InSAR and gravity measurements, *Geology* 37, 63 -66.
721 doi: 10.1130/G25318A.1; 4 figures; 1 table.

722

723 Todesco, M., Rutqvist, J., Pruess, K., Oldenburg, C., 2003b. Multi-phase fluid circulation and
724 ground deformation: a new perspective on bradyseismic activity at the Phlegrean Fields

725 (Italy). In: Proceedings of the 28th Workshop on Geothermal Research Engineering, Stanford,
726 CA, USA.

727

728 Todesco, M., J. Rutqvist, G. Chiodini, K. Pruess and C. M. Oldenburg (2004), Modeling of
729 recent volcanic episodes at Phlegrean Fields Italy: geochemical variations and ground
730 deformation. *Geothermics* 33, 531– 547.

731

732 Walter T.R., R. Wang, V. Acocella, M. Neri, H. Grosser, J. Zschau (2009), Simultaneous
733 magma and gas eruptions at three volcanoes in southern Italy: An earthquake trigger? *Geology*
734 37, 251-254

735

736 Williams S. D. P.(2003), The effect of coloured noise on the uncertainties of rates estimated
737 from geodetic time series. *Journal of Geodesy* 76, 9-10, 483-494.

738

739 **Captions of Figures**

740

741 **Figure 1** – Location of the 2002 gas eruption (DTM from Anzidei et al, 2006) a) Structural
742 sketch map of the Southern Tyrrhenian Sea and Aeolian Islands (After De Astis et al., 2003)
743 (TL Tindari-Letojanni fault system, SA Sisifo-Alicudi fault system). Also shown are the
744 chronology and location of eruptions and earthquakes during late 2002; b) Aerial view of
745 Panarea Island and the archipelago. The arrow indicates the location of major emission point
746 to the SW of Bottaro; c) The gas rose to the sea surface forming bubbles some meters in
747 diameter.

748

749 **Figure 2** – Panarea GPS network. GPS velocities with 1σ uncertainties relative to Panarea
750 reference frame. Fit of four Okada sources (green arrows) and comparison between estimated
751 GPS velocities. a) Anchor IGS sites;. b) Principal axes of the horizontal strain rate tensor and
752 associated 1σ error calculated from relative velocity fields

753

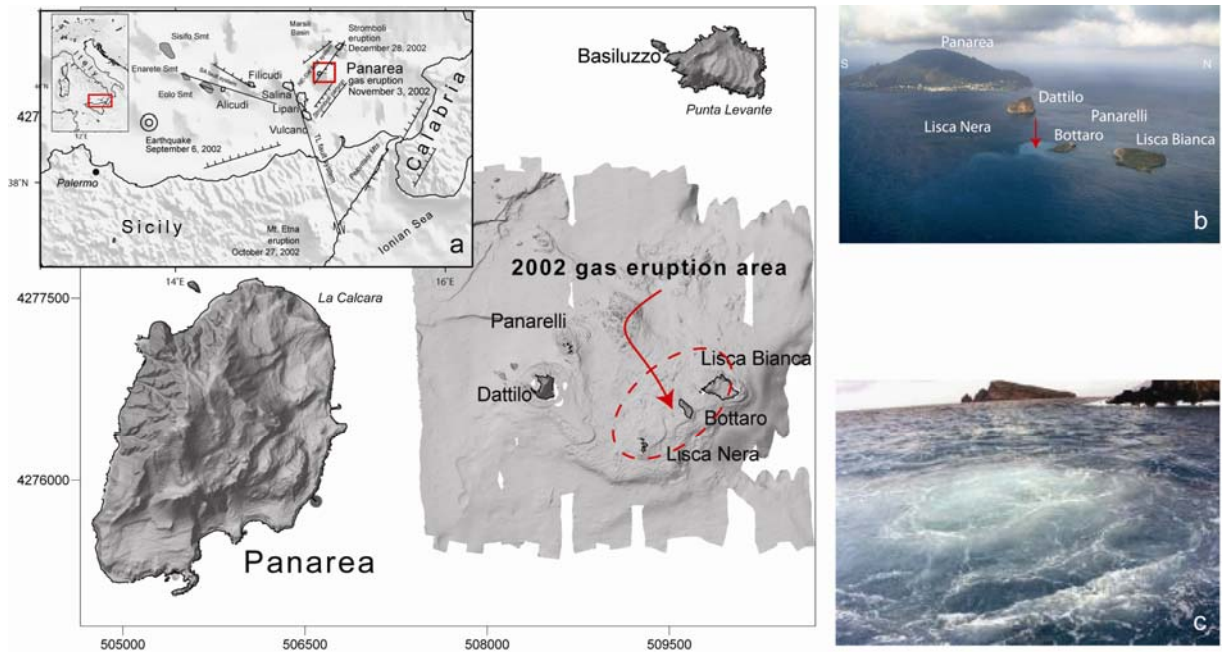
754 **Figure 3** – Coordinate time series of Panarea GPS network relative to Eurasia reference
755 frame. The vertical line represents the estimated step. Formal error 1σ . Inside each box rate is
756 shown. **a)** Coordinate time series of PANA station pre and post 2002 gas eruption in time span
757 1995-2004. PANA time series show a clear offset between 2000 and 2002. **b)** Coordinate time
758 series of the two continuous and the seven non-continuous stations in time span 2002.8 –
759 2007.5. The station of LI3D recorded a horizontal displacement in the middle of 2005 (from
760 June 18th to June 19th)

761

762 **Figure 4** –Conceptual model of Panarea volcano a) projection and section in WNW direction

763 **Figure 5** – Schematic evolution of the Panarea hydrothermal- geothermal system during the
764 1995 – 2007 time span

765



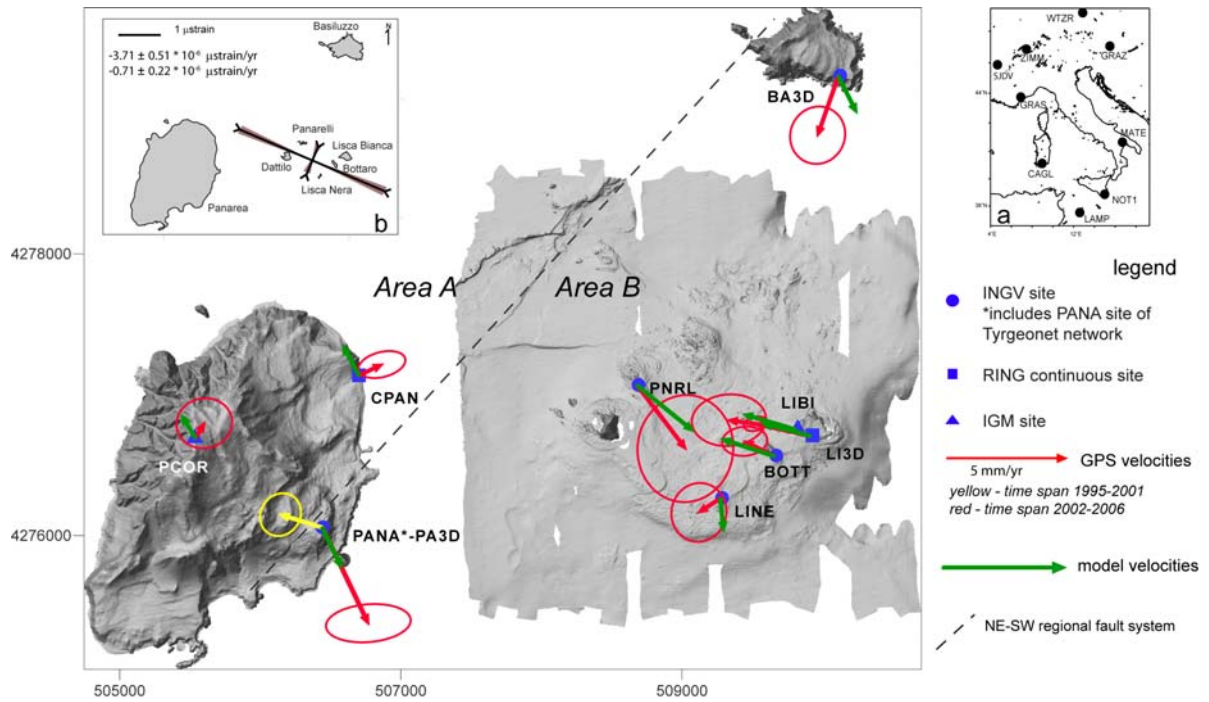
766

767

768 **Figure 1** – Location of the 2002 gas eruption (DTM from Anzidei et al, 2006) a) Structural
769 sketch map of the Southern Tyrrhenian Sea and Aeolian Islands (After De Astis et al., 2003)
770 (TL Tindari-Letojanni fault system, SA Sisifo-Alicudi fault system). Also shown are the
771 chronology and location of eruptions and earthquakes during late 2002; b) Aerial view of
772 Panarea Island and the archipelago. The arrow indicates the location of major emission point
773 to the SW of Bottaro; c) The gas rose to the sea surface forming bubbles some meters in
774 diameter.

775

776



777

778

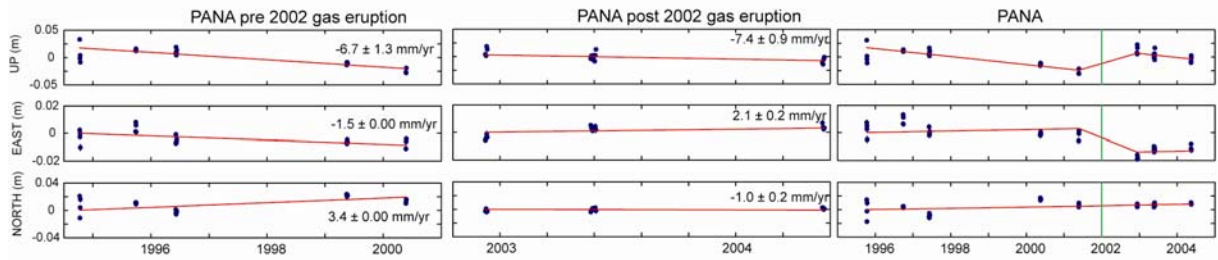
779 **Figure 2** – Panarea GPS network. GPS velocities with 1σ uncertainties relative to Panarea
 780 reference frame. Fit of four Okada sources (green arrows) and comparison between estimated
 781 GPS velocities. a) Anchor IGS sites;. b) Principal axes of the horizontal strain rate tensor and
 782 associated 1σ error calculated from relative velocity fields

783

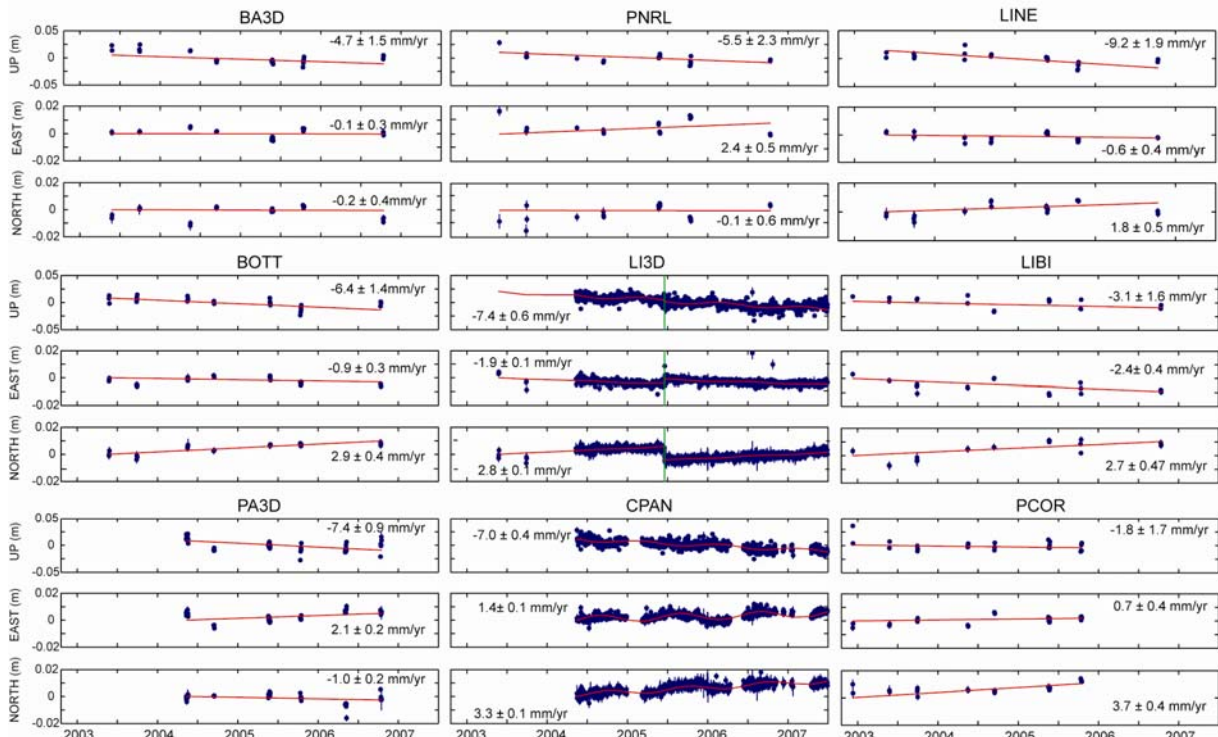
784

785

786



a)



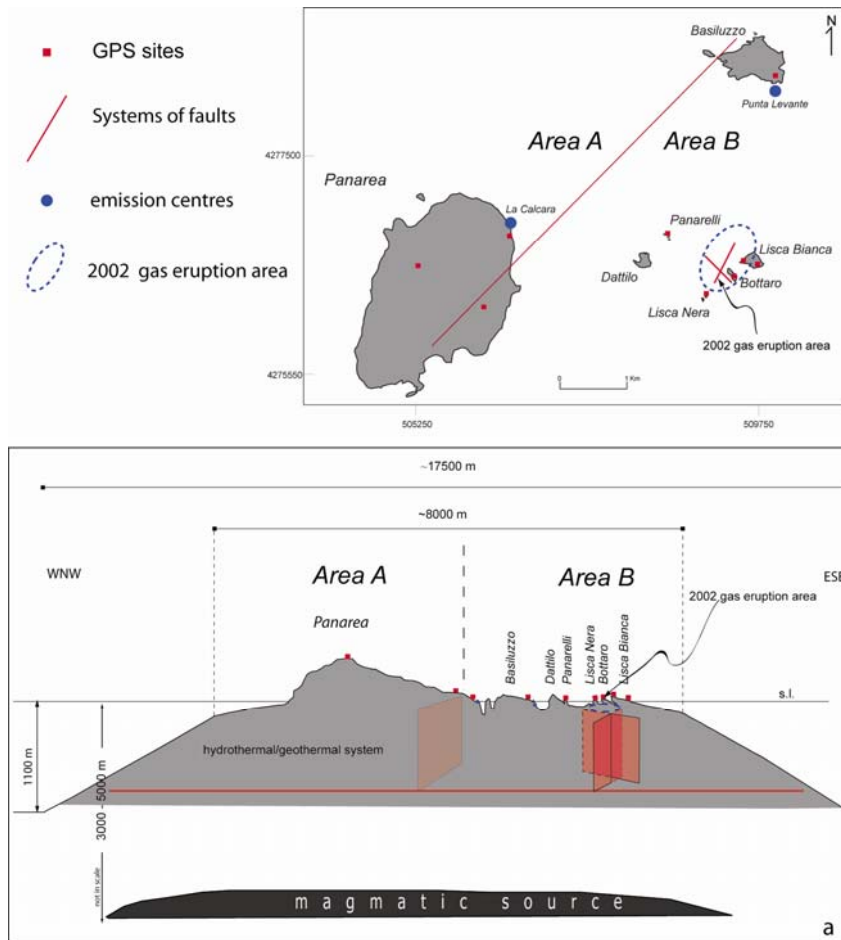
b)

787

788

789 **Figure 3** – Coordinate time series of Panarea GPS network relative to Eurasia reference
 790 frame. The vertical line represents the estimated step. Formal error 1σ . Inside each box rate is
 791 shown. **a)** Coordinate time series of PANA station pre and post 2002 gas eruption in time span
 792 1995-2004. PANA time series show a clear offset between 2000 and 2002. **b)** Coordinate time
 793 series of the two continuous and the seven non-continuous stations in time span 2002.8 –
 794 2007.5. The station of LI3D recorded a horizontal displacement in the middle of 2005 (from
 795 June 18th to June 19th)

796

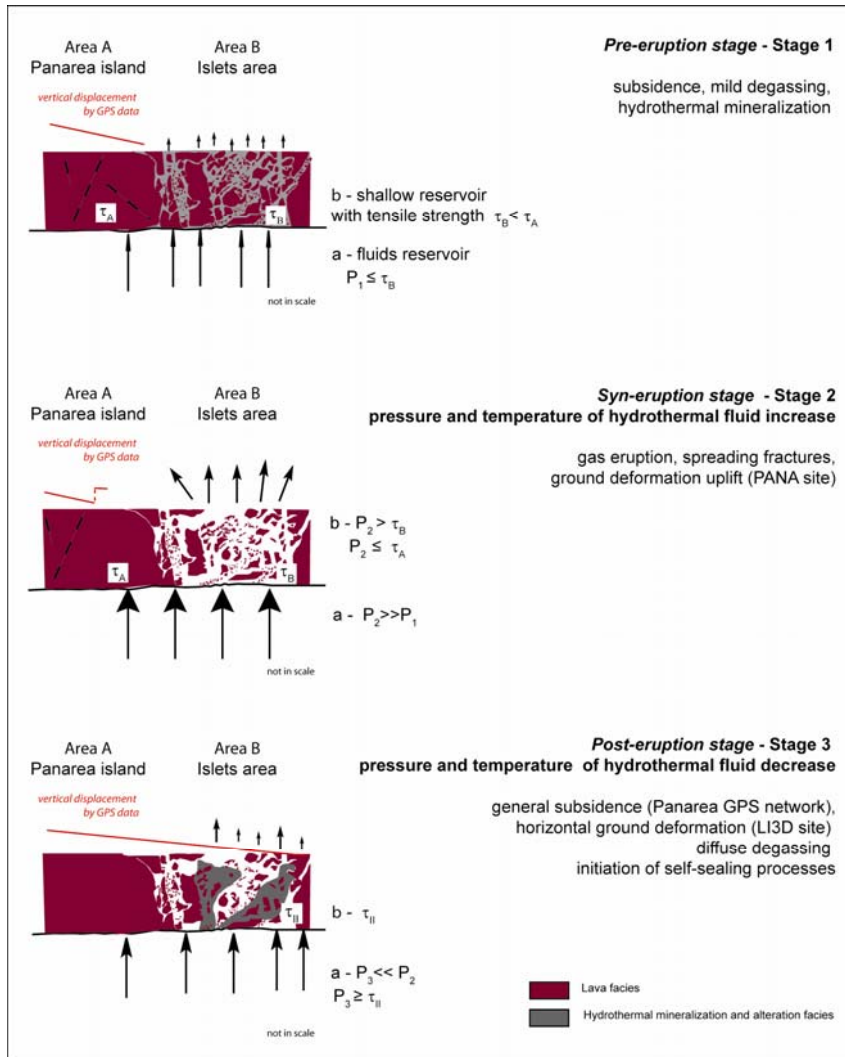


797

798

799 **Figure 4** –Conceptual model of Panarea volcano a) projection and section in WNW direction

800



801

802 **Figure 5** – Schematic evolution of the Panarea hydrothermal- geothermal system during the

803 1995 – 2007 time span

804 **Tables**

Table 1 – Non-continuous stations of Panarea network: observation history, networks

	95	96	97	98	99	00	01	02	03	04	05	06	
1 BA3D								●	●	●	●	●	Panarea
2 BOTT								●	●	●	●	●	Panarea
3 LI3D*								●	●				Panarea
4 LIBI			●					●	●	●	●	●	IGM
5 LINE								●	●	●	●	●	Panarea
6 PA3D									●	●	●	●	Panarea
7 PANA	●	●	●			●	●	●	●	●			Tyrgeonet
8 PCOR								●	●	●	●	●	IGM
9 PNRL								●	●	●	●	●	Panarea

*permanent site from May 2004

● campaign measurements

805

806

807

Table 2 - GPS site positions, Velocities, 1 - □ uncertainties

SITE ID	lon °	lat °	relative to Eurasia					
			East mm/yr	□E mm/yr	North mm/yr	□N mm/yr	Up mm/yr	□Up mm/yr
BA3D	15.116	38.661	-0.1	1.1	-0.2	1.2	-4.7	2.9
BOTT	15.111	38.637	-0.9	0.9	2.9	0.6	-6.4	1.1
CPAN	15.077	38.642	1.3	1.0	3.3	0.6	-7.0	0.9
LI3D	15.114	38.638	-1.9	0.5	2.8	0.3	-7.4	0.4
LIBI	15.113	38.639	-2.4	1.5	2.7	1.1	-3.1	2.4
LINE	15.107	38.634	-0.6	1.1	1.8	1.2	-9.2	2.8
PANA-PA3D	15.074	38.632	2.1	1.7	-1.0	0.8	-7.3	2.7
PCOR	15.064	38.638	0.7	1.1	3.7	1.0	-1.8	3.0
PNRL	15.100	38.641	2.4	2.0	-0.1	2.2	-5.5	5.3

relative to rigid motion of Panarea volcano

SITE ID	lon °	lat °	relative to rigid motion of Panarea volcano					
			East mm/yr	□□ mm/yr	North mm/yr	□□ mm/yr	Up mm/yr	□Up mm/yr
BA3D	15.116	38.661	-0.9	1.1	-2.4	1.2	-4.7	2.9
BOTT	15.111	38.637	-1.2	0.9	0.6	0.6	-6.4	1.1
CPAN	15.077	38.642	0.9	1.0	0.4	0.6	-7.0	0.9
LI3D	15.114	38.638	-2.3	0.5	0.5	0.3	-7.4	0.4
LIBI	15.113	38.639	-2.7	1.5	0.4	1.1	-3.1	2.4
LINE	15.107	38.634	-0.9	1.1	-0.6	1.2	-9.2	2.8
PANA-PA3D	15.074	38.632	1.9	1.7	-3.9	0.8	-7.3	2.7
PCOR	15.064	38.638	0.4	1.1	0.6	1.0	-1.8	3.0
PNRL	15.100	38.641	2.0	2.0	-2.6	2.2	-5.5	5.3

808

809

810

	Horizontal source	NE-SW fault system	NNE fracture system	NW fracture system
Length (m)	infinite	infinite	1100	800
Width (m)	infinite	<i>800</i>	<i>900</i>	<i>800</i>
Depth (m)	<i>900</i>	0	0	0
Azimuth angle (°)	n.a.	45	27	135
Dip angle (°)	0	70	90	90
Rake angle (°)	0	<i>-120</i>	0	0
Slip (cm·yr⁻¹)	0	<i>0.2</i>	0	0
Opening (cm·yr⁻¹)	<i>-0.7</i>	<i>0.3</i>	<i>-0.7</i>	<i>0</i>

811

812 **Table 3** – Best-fit configuration of the four elastic sources. In italic are the parameters
 813 retrieved by non-linear inversion; in bold those constrained by geochemical, volcanological
 814 and structural data. The location of the sources is indicated in Figure 4.

815